NASA TECHNICAL NOTE

NASA TN D-6984

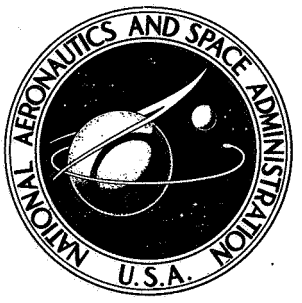

NASA TN D-6984

EFFECTIVE SPECIFIC IMPULSE OF EXTERNAL NUCLEAR PULSE PROPULSION SYSTEMS

by Thaine W. Reynolds

Lewis Research Center

Cleveland, Ohio 44135

NATIONAL AERONAUTICS AND SPACE ADMINISTRATION • WASHINGTON, D. C. • SEPTEMBER 1972

1. Report No. NASA TN D-6984	2. Government Accession No.	3. Recipient's Catalog No.
4. Title and Subtitle EFFECTIVE SPECIFIC IMPULSE OF EXTERNAL NUCLEAR PULSE PROPULSION SYSTEMS		5. Report Date September 1972 6. Performing Organization Code
7. Author(s) Thaine W. Reynolds		8. Performing Organization Report No. E-7013 10. Work Unit No. 112-28
9. Performing Organization Name and Address Lewis Research Center National Aeronautics and Space Administration Cleveland, Ohio 44135		11. Contract or Grant No. 13. Type of Report and Period Covered Technical Note
12. Sponsoring Agency Name and Address National Aeronautics and Space Administration Washington, D.C. 20546		14. Sponsoring Agency Code
15. Supplementary Notes		

16. Abstract

An investigation of a simple self-similar flow model for an external nuclear pulse propulsion system indicates that to achieve the high effective specific impulse of such a system three principal factors are required. They are (1) attaining pulses of optimum energy, (2) attaining good propellant collimation, and (3) using an ablative material for the pusher surface which has high absorptivity for radiant energy at the propellant stagnation temperature.

17. Key Words (Suggested by Author(s))	18. Distribution Statement
Propulsion Specific impulse Thrust	Unclassified - unlimited

19. Security Classif. (of this report)	20. Security Classif. (of this page)	21. No. of Pages	22. Price*
Unclassified	Unclassified	27	$3.00

* For sale by the National Technical Information Service, Springfield, Virginia 22151

EFFECTIVE SPECIFIC IMPULSE OF EXTERNAL NUCLEAR PULSE PROPULSION SYSTEMS

by Thaine W. Reynolds

Lewis Research Center

SUMMARY

A simple self-similar flow model for an external nuclear pulse propulsion scheme has been used to investigate factors affecting the effective specific impulse of such a system. There are three principal factors that control the effective specific impulse: (1) the mean propellant velocity, (2) the fraction of total propellant flow f_c, which intercepts the pusher of the vehicle, and (3) a mass loss factor f_m, which accounts for other mass necessarily ablated from the pusher plate of the vehicle, but which has been assumed herein to contribute little impulse to the vehicle in doing so.

Based on the model used, the following conclusions were drawn:

1. There is an optimum pulse energy for a given system (i.e., a given pusher diameter, and opacity of ablated pusher material) to yield a maximum specific impulse.

2. Increasing the mean propellant velocity does not necessarily result in an increased effective specific impulse for a given system.

3. Mean opacities of 10^3 square meters per kilogram or above appear necessary to approach the achievement of maximum effective specific impulses.

4. Increasing the vehicle size (i.e., increasing pusher diameter) leads to higher values of f_c but lower values of f_m. The resulting effective specific impulse tends to increase if the pulse energy is kept at the optimum value.

INTRODUCTION

The work on the nuclear pulse propulsion scheme proposed initially about 1955 (ref. 1) was carried out under the project name Orion (ref. 2). The original concept involved the use of fission reactions as the energy source. Consequently, the minimum size of the energy package associated with this propulsion scheme was of the order of 4.18×10^{12} joules (1000 tons - TNT equivalent). The corresponding minimum vehicle

size to use these pulse energies effectively is quite large.

There is renewed interest in this mode of propulsion because of the possibility of using small fusion microbombs as the energy source. The fusion reaction might be initiated in small pellets of fusable material by either an intense laser beam (ref. 3) or an intense relativistic electron beam (ref. 4). Nuclear pulse propulsion is of particular interest because of the stated possibility of achieving high thrust-weight ratios at high effective specific impulse values, of the order of 10 000 seconds (ref. 3).

There is no attempt made in this report to evaluate the feasibility of obtaining the fusion reaction by any method. It is assumed that fusion can be attained in any size energy release. This report does consider, however, some basic relations for the propellant flow and heat-transfer problems associated with such a propulsion scheme. A model of the process is used to derive some interrelations between the effective specific impulse and pulse energy size, collimation factor, and mean absorption coefficient of the ablated pusher surface material. The general philosophy with which these calculations were approached was to attempt to estimate upper limits to the effective specific impulse. The assumptions made and values of parameters used are discussed in this vein.

BASIC NUCLEAR PULSE PROPULSION CONCEPT

A schematic diagram showing the use of externally exploded pulse units to propel a space vehicle is shown in sketch (a). A pulse unit containing fusionable material plus

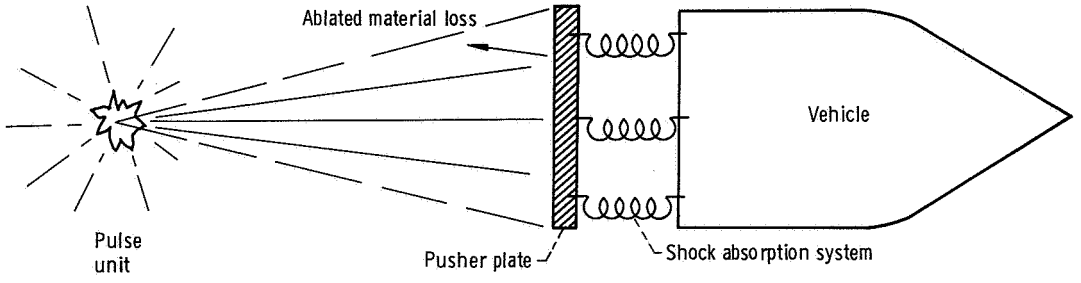

(a)

propellant mass is ejected into position behind the vehicle and the pulse energy triggered. The propellant mass expands. A fraction of the propellant intercepts the pusher plate of the vehicle and transfers momentum and heat to the vehicle. The heat flux causes some ablation of the pusher surface. A succession of such pulses is continued until the desired total impulse for the mission is obtained.

In the usual chemical or electric rocket case, all the propellant mass ejected from

the vehicle contributes its momentum to the vehicle; thus, the effective specific impulse (the impulse per unit weight flow) is a function only of the mean propellant velocity:

$$I_{sp} = \frac{\dot{m}_p \bar{v}}{\dot{w}_p} = \frac{\bar{v}}{g} \tag{1}$$

(All symbols are defined in the appendix.)

As is apparent in sketch (a), not all the mass ejected from the vehicle in the nuclear pulse case is effective in contributing impulse to the vehicle. For the pulse case, the effective specific impulse is

$$(I_{sp})_{eff} = \frac{I(\theta)}{W_p + W_a} \tag{2}$$

where

$$I(\theta) = f_c M_p \bar{v} \tag{3}$$

is the total impulse intercepted by the pusher. The weight of material (other than the propellant) which is lost from the vehicle per pulse and which is assumed to contribute no effective momentum to the vehicle is represented by W_a. In the analysis herein, the only such material considered is material ablated from the pusher plate. The mass loss factor is defined as

$$f_m = \frac{1}{1 + \frac{M_a}{M_p}} \tag{4}$$

The effective specific impulse for the pulse system can thus be expressed as

$$(I_{sp})_{eff} = f_c \cdot f_m \cdot (I_{sp})_{base} \tag{5}$$

where $(I_{sp})_{base} = \bar{v}/g$.

To evaluate the specific impulse for this type of system, then, one has to look at the mean propellant velocity $\bar{v}$ that the system can tolerate, the effectiveness with which the mass of the pulse can be collimated so as to intercept the pusher plate of the vehicle, and the unavoidable mass losses in the system, particularly those lost through interaction of the high velocity propellant with the pusher surface.

The analysis that follows considers the characteristics of the expanding propellant to derive conditions affecting the interaction between the propellant and pusher surface. The principal interactions affecting the performance limitation of the system are the

rate of heat transfer leading to pusher ablation, stress limits on the pusher plate material, and pulse unit design as reflected in the maximum amount of collimation that is attainable. These factors are discussed in the subsequent sections of this report.

SELF-SIMILAR EXPANSION

The propellant mass will be at a high temperature and pressure condition immediately following the pulse energy release. As this material expands into the vacuum of space, some recombinations of ionized and dissociated products will occur. Eventually, through expansion, the density drops to the point where interparticle collisions are relatively unimportant, and the material continues to expand in what is called a "self-similar" manner (ref. 5). The characteristic relation of this type of expansion for the case herein is

$$v(r, t) = \frac{r}{t} \tag{6}$$

In the treatment herein, it is assumed that all the energy absorbed by the propellant mass appears finally as kinetic energy with a Maxwellian distribution about the mean velocity $\bar{v}$:

$$E_p = \frac{1}{2} M_p \bar{v}^2 \tag{7}$$

Also, it is assumed that the condition for collisionless expansion is reached in a relatively short distance, compared to the dimensions of the system, so that the expansion products are effectively emitting from a point source. The adequacy of this assumption is discussed in references 6 to 8.

The density at any location and time is given by (ref. 9)

$$\rho(r, t) = \frac{M_p}{\pi^{3/2} r^3} \left(\frac{v}{\bar{v}}\right)^3 e^{-(v/\bar{v})^2} \tag{8}$$

From equation (8), then, the other properties readily follow:

Mass flow rate per unit area:

$$\dot{m}_p(r, t) = \rho(r, t) \cdot v \tag{9}$$

Pressure:

$$p(r, t) = \rho(r, t)v^2 \tag{10}$$

Energy flow rate per unit area:

$$\dot{E}(r, t) = \frac{\rho(r, t)v^3}{2} \tag{11}$$

If equation (6) is used, the various property relations obtained are as follows:

Property	Equation in terms of M_p	Equation in terms of E_p	Equation	Time at which maximum value occurs	Value at maximum
Density	$\frac{M_p}{\pi^{3/2} r^3}\left(\frac{t_r}{t}\right)^3 e^{-(t_r/t)^2}$	$\frac{2E_p}{\pi^{3/2} r^3 \bar{v}^2}\left(\frac{t_r}{t}\right)^3 e^{-(t_r/t)}$	(12)	$t_m = 0.817\left(\frac{r}{\bar{v}}\right)$	$\rho_m = 0.147\frac{E_p}{r^3\bar{v}^2}$
Mass flow/area	$\frac{M_p\bar{v}}{\pi^{3/2} r^3}\left(\frac{t_r}{t}\right)^4 e^{-(t_r/t)^2}$	$\frac{2E_p}{\pi^{3/2} r^3 \bar{v}}\left(\frac{t_r}{t}\right)^4 e^{-(t_r/t)^2}$	(13)	$t_m = 0.707\left(\frac{r}{\bar{v}}\right)$	$\dot{m}_m = 0.194\frac{E_p}{r^3\bar{v}}$
Pressure	$\frac{M_p\bar{v}^2}{\pi^{3/2} r^3}\left(\frac{t_r}{t}\right)^5 e^{-(t_r/t)^2}$	$\frac{2E_p}{\pi^{3/2} r^3}\left(\frac{t_r}{t}\right)^5 e^{-(t_r/t)^2}$	(14)	$t_m = 0.633\left(\frac{r}{\bar{v}}\right)$	$p_m = 0.291\frac{E_p}{r^3}$
Energy flow/area	$\frac{M_p\bar{v}^3}{2\pi^{3/2} r^3}\left(\frac{t_r}{t}\right)^6 e^{-(t_r/t)^2}$	$\frac{E_p\bar{v}}{\pi^{3/2} r^3}\left(\frac{t_r}{t}\right)^6 e^{-(t_r/t)^2}$	(15)	$t_m = 0.577\left(\frac{r}{\bar{v}}\right)$	$E_m = 0.241\frac{E_p\bar{v}}{r^3}$

Some plots of equations (12) to (15) are shown in figure 1 for a particular E_p/r^3 value. The time scales are nondimensional in this figure, the reference time being $t_r = r/\bar{v}$. One can note, then, that the time at which the maxima in the various parameters occur (t_m) is a direct function of the separation distance r. Also, the total time of pulse interaction is of the order of three times t_m, so that pulse interaction time also varies directly with separation distance. This fact has a bearing on the heat-transfer effects as will be seen later.

Consider the arrival of propellant from a pulse onto a plane normal to the main flow direction (sketch (b)). The mass flux at point (z, β) normal to the plane is

$$\rho(z, \beta) \cdot v \cos \beta = \frac{M_p\bar{v} \cos \beta}{\pi^{3/2} r^3}\left(\frac{v}{\bar{v}}\right)^4 e^{-(v/\bar{v})^2} \tag{16}$$

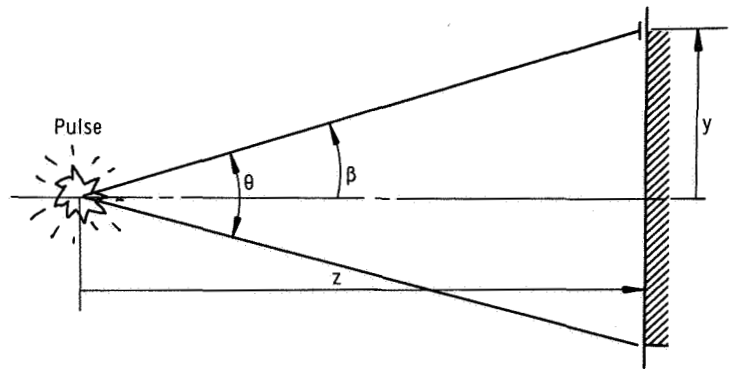

(b)

and the pressure on the plane at that point is

$$p(z, \beta) = \frac{M_p \bar{v}^2 \cos^2\beta}{\pi^{3/2} r^3} \left(\frac{v}{\bar{v}}\right)^5 e^{-(v/\bar{v})^2} \tag{17}$$

Typical radial variations of pressure and density are shown in figure 2. The impulse per unit area on the plane at (z, β) in the z-direction is

$$I(\beta) = \frac{M_p \bar{v} \cos^2\beta}{2\pi^{3/2} r^2} \tag{18}$$

The total impulse in the z-direction from flux within a given cone angle θ is

$$I(\theta) = \frac{2}{\sqrt{\pi}} M_p \bar{v} \sin^2\left(\frac{\theta}{4}\right) \cos^2\left(\frac{\theta}{4}\right) \tag{19}$$

But the fraction of the total mass flow which is included within a given cone angle θ is

$$f_\theta = \sin^2\left(\frac{\theta}{4}\right) \tag{20}$$

for isotropic distribution. Thus, considering only the propellant interception factor, the effective specific impulse of a system using a circular pusher plate to intercept the mass flow within a cone angle θ is

$$(I_{sp})_{eff} = \frac{I(\theta)}{M_p g} = \frac{2}{\sqrt{\pi}} \cos^2\left(\frac{\theta}{4}\right) f_\theta \cdot \frac{\bar{v}}{g} \tag{21}$$

If a pulse unit is designed to direct a disproportionate fraction of the total mass into a given cone angle, the flow is still assumed uniformly distributed within the cone. The parameter C (hereafter referred to as a collimation factor) is defined as the ratio of the enhanced total mass in the cone to the amount in the cone if the distribution were isotropic. It can be expressed as

$$C = \frac{f_\theta}{\sin^2\left(\frac{\theta}{4}\right)} \tag{22}$$

With this assumption of the flow distribution, the relations developed for the isotropic distribution may be used for collimated flow cases by replacing the propellant mass term M_p with the product $C\,M_p$.

If the case with collimated flow is now assumed, the relation for total impulse (eq. (19)) is put in terms of pulse energy $E_p\left(=\frac{1}{2} M_p \bar{v}^2\right)$ and C:

$$I(\theta) = \frac{4}{\sqrt{\pi}} \cos^2\left(\frac{\theta}{4}\right) \sin^2\left(\frac{\theta}{4}\right) \frac{CE_p}{\bar{v}} \tag{23}$$

The pressure is highest at the center of the plate ($\beta = 0$):

$$p(z, t) = \frac{2CE_p}{\pi^{3/2} r^3} \left(\frac{t_r}{t}\right)^5 e^{-(t_r/t)^2} \tag{24}$$

At $\beta = 0$, the maximum pressure at any time is

$$p_m = 0.291 \frac{CE_p}{r^3} \tag{25}$$

The effect of two factors (equivalent energy of the pulse and attainable collimation factor) involved in the design of pulse units on the attainable propellant interception factor f_c can be seen by the following development. Combining equations (21) and (23) yields

$$\frac{(I_{sp})_{eff}}{(I_{sp})_{base}} = \frac{C}{2\sqrt{\pi}} \sin^2\left(\frac{\theta}{2}\right) \tag{26}$$

In all subsequent relations where a specific value of maximum pressure is used, a value of $p_m = 6.9 \times 10^8$ newtons per square meter (equivalent to about 100 000 psi) is used.

This value represents a reasonable upper limit to the allowable yield stress of materials that might be used for the pusher. If this value is used, equation (25) becomes

$$r_{min} = 7.51\times10^{-4}(CE_p)^{1/3} \tag{27}$$

The pusher diameter required to intercept the flux in a given cone angle θ is obtained from the geometric relation (shown in sketch (c)).

$$\sin\left(\frac{\theta}{2}\right) = \frac{\frac{d}{2}}{\sqrt{r^2 + \left(\frac{d}{2}\right)^2}} \tag{28}$$

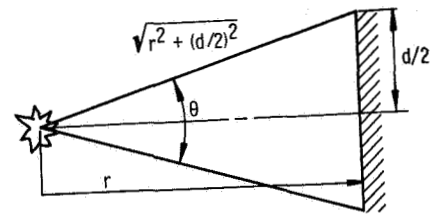

(c)

Combining equations (26) to (28) yields the relation

$$f_c = \frac{C}{2\sqrt{\pi}}\left[\frac{d^2}{d^2 + 2.26\times10^{-6}(CE_p)^{2/3}}\right] \tag{29}$$

With the assumption that all the propellant mass has the mean velocity $\bar{v}$, the upper limit to f_c is 0.5 in order to satisfy the momentum balance requirement. Equation (29), with the upper limit restriction of 0.5 for f_c, is shown plotted in figure 3 for four values of total pulse energy, $E_p = 4.18\times10^9$, 4.18×10^{10}, 4.18×10^{11}, and 4.18×10^{12} joules (1, 10, 100, and 1000 ton equivalents). (For reference, 1 gram of deuterium-tritium (DT) mixture fully reacted is equivalent to about 3.344×10^{11} joules (80 tons TNT).) The interrelation among vehicle size (as reflected by pusher diameter), pulse energy size (E_p) and pulse unit design (as reflected by the collimation factor C) is evident.

When the separation distance is maintained at the smallest value permitted by pressure limitations (the conditions imposed for fig. 3), one can note that there is a large improvement in the propellant interception factor f_c for (1) better collimation of the

propellant, (2) smaller energy pulse value for the same degree of collimation, and (3) larger size vehicles (i.e., larger pusher diameters).

PROPELLANT-PUSHER INTERACTION

When the flux of propellant arrives at the pusher plate, the initial, high velocity particles cause some sputtering. Some penetration into the material of the pusher also occurs. The effect of this initial bombardment is small compared to the eventual ablation caused by the arrival of the remainder of the pulse mass. The propellant that arrives is assumed to just lose its kinetic energy and form a hydrodynamic stagnation layer. The temperature of this stagnation layer is calculated by assuming that it reaches equilibrium through blackbody radiation back to the vacuum of space.

Thus, when the energy flow rate relation (15) is used, the equilibrium can be expressed as

$$\sigma T_s^4 = \frac{E_p \bar{v}}{\pi^{3/2} r^3} \left(\frac{t_r}{t}\right)^6 e^{-(t_r/t)^2} \tag{30}$$

or

$$T_s = \left[\frac{E_p \bar{v}}{\pi^{3/2} \sigma r^3} \left(\frac{t_r}{t}\right)^6 e^{-(t_r/t)^2}\right]^{1/4} \tag{31}$$

A plot of this relation is shown in figure 4. Stagnation temperatures up to the 20-electron-volt range are typical.

The formation of this high temperature layer causes the temperature of a pusher surface to rise quickly to the ablation level. The ablated gas then forms a protective layer and slows down subsequent ablation rates.

At the temperature levels of the stagnation layer of gas, heat transfer to the pusher is mainly by radiation. Therefore, a surface material whose ablated products have a high absorptance for radiation in the frequency range characteristic of the temperature of the stagnation layer would be a distinct advantage in limiting ablation amounts. This situation is similar to that encountered in the gas-core nuclear rocket (refs. 10 and 11).

In order to estimate the magnitude of the heat-transfer problem, the model of the interaction process shown in sketch (d) was assumed. The ablated vapor layer and the high-temperature layer from stagnating propellant were assumed to remain unmixed. The flow of heat through the ablated vapor layer was then looked at as a combined pro-

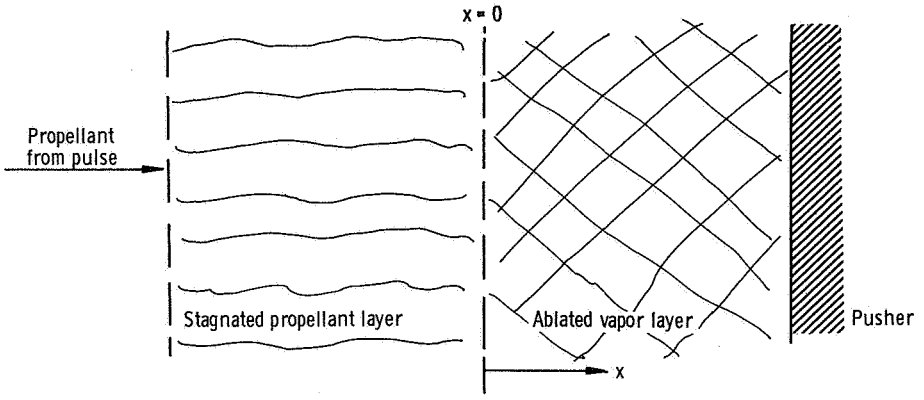

(d)

cess of radiation and conduction. It is assumed that the ablated vapor, of necessity, will be of material which has a high absorptance for radiant energy at the temperature of the stagnation layer. The one-dimensional equation describing the transfer of heat in an optically thick radiative-conductive medium with no heat source terms is

$$\frac{4\sigma}{3a_R}\frac{\partial^2 T^4}{\partial x^2} + k_c \frac{\partial^2 T}{\partial x^2} = \rho c_p \frac{\partial T}{\partial t} \tag{32}$$

where a_R is the adsorptance of vapor layer and k_c the thermal conductivity of vapor layer.

Numerical solutions to equation (32) may be obtained by assuming a boundary temperature history at $x = 0$ (given by the stagnation temperature relation (31)) and with the temperature gradient approaching zero as x becomes large. Typical temperature profiles for these solutions are shown in figure 5. The rate of advance of the temperature "front" into the ablated vapor medium is also obtained.

The inflection point of the temperature-distance relation occurs at about the temperature level for which equal rates of heat transfer occur by both radiation and conduction modes. This condition is given approximately by

$$\frac{16\sigma T^3}{3a_R} = k_c \tag{33}$$

This relation becomes

$$T_{eV} = 0.0128(a_R k_c)^{1/3} \equiv 0.0128\left[\left(\frac{a_R}{\rho}\right)\rho k_c\right]^{1/3} \tag{34}$$

when substituting for σ and expressing temperature in electron volt units. The temperature level of the major portion of the ablated medium is below this inflection point temperature. This observation is noted here because of its relation to the properties of the ablated layer.

The assumption that most of the radiant energy from the stagnation layer is absorbed in a relatively small thickness of the ablated vapor leads to the temperature profiles noted in figure 5, that is, a relatively steep temperature front that propagates through the medium. The similarity here to the gas-core rocket profiles is noted (refs. 10 and 11). In the gas-core case, seeded gas is fed toward the advancing temperature front at such a rate as to maintain the steep temperature profile away from the wall of the rocket chamber. In the pusher case herein, ablated material is fed into the vapor state at a rate governed by the amount of heat that reaches the wall and the amount of energy required to vaporize plate material and raise it to the temperature level of the ablated medium.

In the following calculation of the amount of pusher ablation, it is assumed that heat transfer to the surface by radiation (though only a small fraction of the total radiant energy available) is still the major mode of energy transfer. The incremental heat transfer per unit area, then, is

$$dQ = \sigma T_s^4(t) e^{-a_R x(t)}\, dt \tag{35}$$

The increment of mass ablated per unit area is

$$dm_a = \rho\, dx = \frac{dQ}{H_a} \tag{36}$$

Equations (35) and (36) were solved numerically for energy input using equation (30) when no ablated layer ($x = 0$) was present at $t = 0$ and when any decrease in $x(t)$ resulting from propagation of the temperature front into the ablated medium was neglected. The calculated ablation amounts will thus be lower than actual because of this latter assumption.

Typical total ablation per unit area values are shown in figure 6. These were calculated using a value of 5×10^7 joules per kilogram for H_a. The total ablation amount, however, is not especially sensitive to H_a as shown in figure 7. A factor of 10 change in H_a causes only a 15 to 20 percent change in the total ablation amount under the conditions of these calculations. Figure 8 shows the range of energy absorption that goes into just ionization and thermal energy of the species for two metal vapors, iron (Fe) and uranium (U). Sublimation energy is, of course, also included in H_a.

The effect of separation distance on ablation rates is shown in figure 9 by a comparison of curves. As the separation distance is increased, the energy arrival rate (per unit

area) decreases. However, the total interaction time increases. The net effect (fig. 9) of increasing the separation distance to four times the minimum separation distance (eq. (28)) was to decrease the total ablation by only about 32 percent at $E_p = 4.18\times10^{12}$ joules (1000 tons) and 38 percent at $E_p = 4.18\times10^{9}$ joules (1 ton).

The ablation calculations shown up to this point have been for conditions at the center of the pusher ($\beta = 0$). Away from the center ($\beta > 0$), the ablation decreases as shown in figure 10. The same countering influence of the two factors, energy intensity and interaction time, are present in the radial variation as in the separation distance variation (fig. 9). For $E_p = 4.18\times10^{9}$ joules (1 ton), a 17 percent decrease in the ablation rate was calculated at 45° off the axis.

Of special interest now is a calculation of the mass loss factor f_m. Since the only such loss considered herein is that by means of ablation from the pusher surface, f_m is given by equation (4).

A cylindrical pusher plate of diameter d (sketch (e))

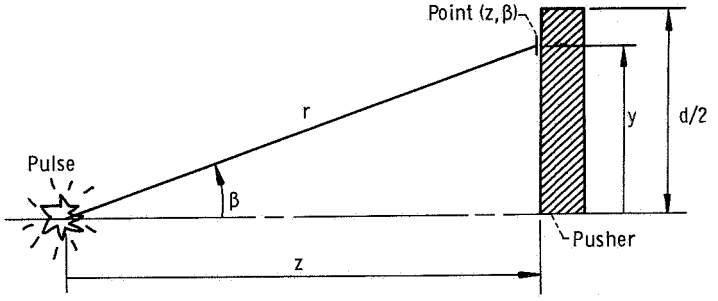

(e)

is now considered. The ratio of total ablation per pulse to propellant mass for the pusher plate of diameter d is

$$\frac{M_a}{M_p} = \frac{2\pi}{M_p}\int_0^{d/2} y\left[\int_0^{\infty}\frac{\dot{E}_i(z,\beta)}{H_a}\,e^{-a_R x}\,dt\right]dy \tag{37}$$

The energy arrival rate at (z,β) for a pulse with collimation factor C is

$$\dot{E}_i(z,\beta) = C\rho(z,\beta)\frac{v_z^3}{z} \tag{38}$$

Now, let $t_z = z/\bar{v}$. Then $t_r = t_z \sec\beta$ and, using equation (16),

$$\dot{E}_i(z,\beta) = \frac{CE_p\bar{v}}{\pi^{3/2}z^3}\left(\frac{t_z}{t}\right)^6 e^{-\left(\frac{t_z}{t\cos\beta}\right)^2} \tag{39}$$

At this point the calculations are restricted to values of z corresponding to the maximum pressure limitation (eq. (27)). When equation (27) is used, equation (39) becomes

$$\dot{E}_i(z,\beta) = 4.23\times10^8\,\bar{v}\left(\frac{t_z}{t}\right)^6 e^{-\left(\frac{t_z}{t\cos\beta}\right)^2} \tag{40}$$

Equation (37) is transformed to

$$\frac{M_a}{M_p} = \left(\frac{10\pi\bar{v}^2}{E_p}\right)\int_0^{d/2} y\left[\int_0^{\infty}\frac{4.23\times10^7}{H_a}z_m\left(\frac{t_z}{t}\right)^6 e^{-\left(\frac{t_z}{t\cos\beta}\right)^2} e^{-a_R x}\, d\left(\frac{t}{t_z}\right)\right]dy \tag{41}$$

by using the previous relations and putting the pulse energy in terms of E_p.

The inner integral (with respect to t/t_z) was solved numerically under the same assumptions as used in solving equations (35) and (36). The resulting values of the mass loss factor f_m for several combinations of variables are shown in figure 11. The curves stop at the limiting diameter where the propellant interception factor is 0.5.

The larger the pusher diameter, the smaller is the factor f_m, other factors being constant. More pusher area is exposed to ablating conditions, while pulse mass M_p remains constant. The mass ablation loss factor is lower for smaller energy pulses for the same size pusher plate. This is because the separation distance z_m is lower for lower energy pulses, and the pusher intercepts a greater fraction of the total energy flux from the pulse.

The absorption coefficient a_R/ρ has a marked effect on the mass loss factor since, as was noted before (fig. 6), the total ablation amount is nearly inversely proportional to a_R/ρ for the conditions of these calculations.

SPECIFIC IMPULSE

A simplified model of the overall processes involved in the external nuclear pulse propulsion scheme has been assumed. Only the features of the propulsion system that affect the overall or effective specific impulse have been considered. The propellant

flow from the pulse energy source has been assumed to occur self-similarly from a point source. A collimation factor has been used to account for the concentration of more propellant into smaller flow cone angles than would occur simply from isotropic expansion. The hydrodynamic stagnation layer temperature is determined by the balance between incoming kinetic energy and blackbody radiation back to space. Ablation of pusher surface material occurs by radiant heat transfer from the stagnation temperature through the ablated layer. A mean opacity for the ablated layer material is assumed.

Using this model, two principal factors determining the effective specific impulse were calculated: the propellant loss factor f_c (eq. (29) and fig. 3), and the mass loss factor f_m (eq. (4) and fig. 11). These two factors are combined to yield the ratio

$$(I_{sp})_{eff} = f_c \cdot f_m \cdot (I_{sp})_{base} \tag{42}$$

Some typical plots of relation (42) are shown in figure 12 for a collimation factor of 3 and a_R/ρ value of 10^2 square meters per kilogram. It is apparent in this figure that the optimum specific impulse for smaller pusher diameters is attained with the small pulse energies. Under the conditions of figure 12 there is little or no improvement in effective specific impulse in going to higher mean propellant velocities at the smaller pulse energy levels.

CONCLUDING REMARKS

The calculation of effective specific impulse by the model used herein is felt to be optimistically high for a number of reasons. Most of the assumptions made relative to the calculation of the amount of ablation yield results believed to be lower than the true amount. Some examples are the following:

(1) The value of H_a used (5×10^7 J/kg) is at the high end of the expected range of values (fig. 8).

(2) The total heat transfer to the surface is greater than or equal to the radiant transfer portion assumed.

(3) The decrease in $\rho\bar{x}$ caused by the thermal wave propagation into the ablated medium is neglected in the exponential factor $e^{-(a_R/\rho)\rho\bar{x}}$.

(4) Mass loss other than the ablated amount M_a may occur.

The assumption of uniform distribution of propellant mass in the case of collimated flow leads to propellant interception factors that are higher than would be obtained for a more probable distribution. One would expect that in collimated flow mass would be more concentrated along the axis ($\beta = 0$). Thus, the stipulation of a maximum pressure limitation would mean that a greater separation distance would be required. This, then, would lead to lower f_c values for a given pulse energy and pusher diameter. However,

the assumption that no impulse is contributed by the ablated vapor or by reexpansion of the stagnation layer leads to specific impulse values that are lower than the real case.

The principal variables affecting the performance of the system are the following: E_p, the size of the energy pulse; r, the separation distance between the pulse and the pusher; $\bar{v}$, the mean propellant velocity; C, the collimation factor; a_R, the mean opacity of the ablated vapor; β, the angle from the pulse-pusher centerline; and H_a, the energy absorbed during ablation. The effect of variations in these variables on the effective specific impulse of a given system is now discussed. The term "given system" is used here to mean one of constant diameter and a_R/ρ value.

(1) Pulse energy, E_p. There is an optimum pulse energy to yield the maximum effective specific impulse with a given vehicle size (fig. 12). This result assumes that the separation distance is always kept at the minimum dictated by pressure limitation. The propellant interception factor increases (fig. 3) with decreased pulse energy. The total ablation amount decreases with smaller E_p (fig. 6); however, the ratio of the total ablation to the total propellant flow is greater at smaller E_p. Thus, the mass loss factor is lower at lower E_p values (fig. 11).

(2) Separation distance, r. For a given pulse energy, locating the pusher farther from the pulse source cuts total ablation but not greatly (fig. 8). The decrease in energy arrival rate is counteracted by the increased interaction time. The big effect of r is, of course, a geometric one; that is, the greater the separation distance, the larger the required pusher diameter to intercept the same flux from the pulse.

(3) Mean propellant velocity, $\bar{v}$. There is no change in pressure with a change in $\bar{v}$; the pressure is a function of the parameter CE_p/r^3. However, the pulse energy required for a given total impulse is directly proportional to $\bar{v}$.

There is no effect on total ablation with $\bar{v}$ in this model. While the energy arrival rate is proportional to $\bar{v}$, the interaction time is inversely proportional to $\bar{v}$; hence, the effects on total ablation exactly cancel. This result is obtained because the absorptance a_R/ρ has been treated as a constant, independent of frequency. However, in a real system, the absorptance is a function of frequency (and hence the temperature of the radiation source). Some effect of $\bar{v}$ on ablation would be expected in such cases.

(4) Collimation factor, C. The collimation factor, which has a marked effect on the propellant interception factor (fig. 3), is a problem associated with the pulse unit design. Thus, no estimate of the range of possible values is attempted here. A value of $C = 3$ has been used herein for illustration purposes, but no implication about the probable attainment of this value is intended.

(5) Rosseland mean opacity of ablated vapor, a_R. This parameter is one of the most important ones affecting pusher ablation. The ratio of total ablated material to total propellant is nearly inversely proportional to a_R/ρ under the conditions of interest herein. The importance of this property to the performance of the system makes the

selection of an ablating material and the correct determination of its a_R of greatest impact.

In the simplified approach of the model used, it was assumed that a_R/ρ was constant. Experimental values of opacity of materials under the conditions of temperature and pressure encountered in the nuclear pulse interaction are not readily available for many materials. Some plots of the variation of the Rosseland mean opacity for several materials are shown in figures 13 and 14 (refs. 12 to 14).

One can note by a comparison of figures 1 and 5 that most of the ablation has occurred considerably before the peak pressure (restricted to 6900 atm) is attained. The range of a_R/ρ values indicated for materials in figures 13 and 14 would be generally below 10^3 square meters per kilogram during most of the ablation process.

The use of a mean opacity value independent of frequency (hence independent of the temperature of the radiating source) in calculating ablation rates undoubtedly leads to some inaccuracies in conclusions, as pointed out in item (3). The results of the analysis do, however, serve to establish the required range for the opacity at operating conditions in order that total ablation amounts will be kept within an acceptable range. Whether this range of a_R values can be achieved with otherwise suitable pusher surface materials is an area requiring much more detailed consideration.

(6) Angular variation, β. There is considerable variation in the flow properties (such as pressure, density, etc.) from the center of a pusher to the edge (fig. 2). At the time the peak pressure occurs at the center ($\beta = 0$), the pressure at 30^o off center is about 0.55 times the peak value. The variation with β is greater than this at times prior to the occurrence of the peak value, and is less than this at times after the peak values have been reached. These time and radius variations in the pressure, for instance, undoubtedly complicate the pusher design to withstand the accompanying corresponding stresses encountered.

(7) Energy absorbed during ablation, H_a. An increase in H_a decreases the total ablation as expected, but not nearly in direct proportion (fig. 6). At a pulse energy E_p of 4.18×10^9 joules (1 ton), for example, an increase in H_a of a factor of 10 caused only a 15 to 20 percent decrease in total ablation.

Lewis Research Center,
National Aeronautics and Space Administration,
Cleveland, Ohio, July 26, 1972,
112-28.

APPENDIX - SYMBOLS

a_R	Rosseland mean opacity, m^{-1}
C	collimation factor
c_p	heat capacity, J/(m)(sec)(K)
d	pusher diameter, m
E	energy, J
E_p	pulse energy, J (1 ton TNT $\equiv 4.18\times10^9$ J)
$\dot{E}$	energy arrival rate, J/m^2 sec
$\dot{E}_i$	energy arrival rate at interface, x = 0 (see sketch (d)), $J/(m^2)(sec)$
f_c	fraction of pulse mass that intercepts pusher
f_m	ablation mass loss factor, defined in eq. (4)
f_θ	fraction of total mass flow that is included within cone angle, θ
g	gravitational acceleration, m/sec^2
H	enthalpy, J/kg
H_a	energy required to ablate pusher material, J/kg
$I(\beta)$	impulse per unit area in z-direction at angle β, $N\text{-}sec/m^2$
$I(\theta)$	total impulse in z-direction within included angle, θ, N-sec
I_{sp}	specific impulse, sec
$(I_{sp})_{base}$	base specific impulse, $\bar{v}/g$, sec
$(I_{sp})_{eff}$	effective specific impulse, sec
k_c	thermal conductivity, J/(m)(sec)(K)
M_a	total mass ablated from pusher per pulse, kg
M_p	propellant mass per pulse, kg
m_a	mass per unit area ablated from pusher, kg/m^2
$\dot{m}_p$	propellant flow rate per unit area, $kg/(m^2)(sec)$
p	pressure, N/m^2 (1 atm = 1.013×10^5 N/m^2)
p_m	maximum pressure, N/m^2
Q	heat transferred per unit area, J/m^2
r	radius, distance from pulse center, m

r_{min}	minimum radius, m
T	temperature, K
T_{eV}	stagnation temperature, eV
T_s	stagnation temperature, K
t	time after pulse initiation, sec
t_m	time at which maximum value occurs, sec
t_r	reference time, $r/\bar{v}$, sec
t_z	reference time, $z/\bar{v}$, sec
V_i	ionization potential, eV
v	velocity, m/sec
v_z	z-component of velocity, m/sec
$\bar{v}$	mean propellant velocity, m/sec
W_a	weight of material ablated per pulse, N
W_p	weight of propellant per pulse, N
$\dot{w}_p$	propellant weight flow per unit area, $kg/(m)(sec^3)$
x	thickness of ablated layer, m
y	distance from $\beta = 0$ line in plane perpendicular to z, m
z	distance, pulse center to pusher plane, m
z_m	minimum separation distance from pressure limitation, m
β	angle from centerline
θ	included cone angle
ρ	density, kg/m^3
ρ_m	maximum density, kg/m^3
σ	Stefan-Boltzmann constant, W/m^2K^4

REFERENCES

1. Everett, C. J.; and Ulam, S. M.: On a Method of Propulsion of Projectiles by Means of External Nuclear Explosions. Rep. LAMS-1955, Los Alamos Scientific Lab., Aug. 1955.

2. Nance, J. C.: Nuclear Pulse Propulsion. IEEE Trans. on Nucl. Sci., vol. NS-12, no. 1, Feb. 1965, pp. 177-182.

3. Boyer, Keith; and Balcomb, J. D.: System Studies of Fusion Powered Pulsed Propulsion Systems. Paper 71-636, AIAA, June 1971.

4. Winterberg, F.: Rocket Propulsion by Thermonuclear Micro-Bombs Ignited with Intense Relativistic Electron Beams. Raumfahrtforschung, vol. 15, no. 5, Sept./Oct. 1971, pp. 208-217.

5. Sedov, Leonid I.: Similarity and Dimensional Methods in Mechanics. Academic Press, 1959.

6. Molmud, Paul: Expansion of a Rarefied Gas Cloud into a Vacuum. Phys. Fluids, vol. 3, no. 3, May-June 1960, pp. 362-366.

7. Greenspan, H. P.; and Butler, D. S.: On the Expansion of a Gas into Vacuum. J. Fluid Mech., vol. 13, pt. 1, May 1962, pp. 101-119.

8. Mirels, H.; and Mullen, J. F.: Expansion of Gas Clouds and Hypersonic Jets Bounded by a Vacuum. AIAA J., vol. 1, no. 3, Mar. 1963, pp. 596-602.

9. Narasimha, Roddam: Collisionless Expansion of Gases into Vacuum. J. Fluid Mech., vol. 12, pt. 2, Feb. 1962, pp. 294-308.

10. Ragsdale, Robert G.; and Willis, Edward A., Jr.: Gas-Core Rocket Reactors - A New Look. Paper 71-641, AIAA, June 1971.

11. Ragsdale, Robert G.: Status of Open-Cycle Gas-Core Reactor Project Through 1970. NASA TM X-2259, 1971.

12. Bernstein, Jeremy; and Dyson, Freeman J.: The Continuous Opacity and Equations of State of Light Elements at Low Densities. Rep. GA-848, General Dynamics Corp., July 13, 1959.

13. Bernstein, Jeremy; and Dyson, Freeman J.: The Opacities and Equations of State of Some Mixtures of Light Elements. Rep. GAMD-865, General Dynamics Corp., July 6, 1959.

14. Patch, R. W.: Status of Opacity Calculations for Application to Uranium-Fueled Gas-Core Reactors. Research on Uranium Plasmas and Their Technological Applications. NASA SP-236, 1971, pp. 165-171.

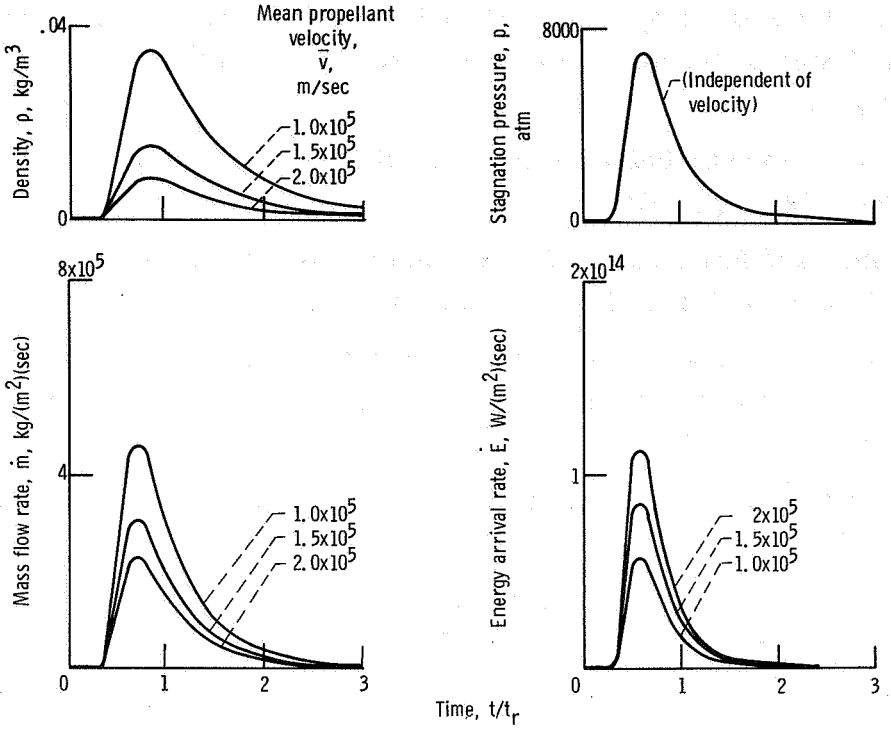

Figure 1. - Time variation of conditions at pusher location E_p/r^3 of 2.37×10^9 joules per cubic meter.

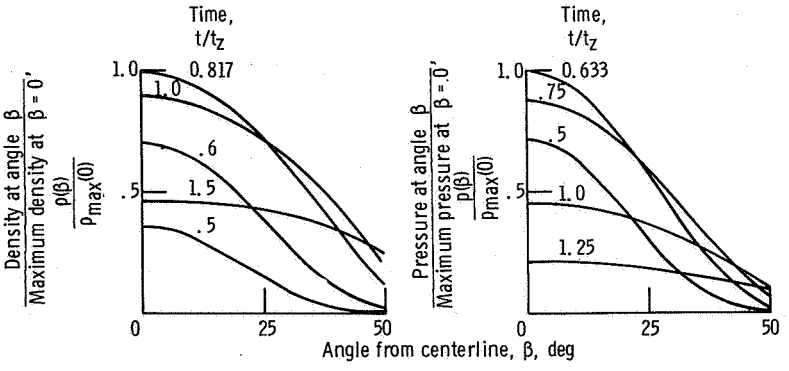

(a) Density, ρ. (b) Pressure, p.

Figure 2. - Radial variation of properties on pusher plate.

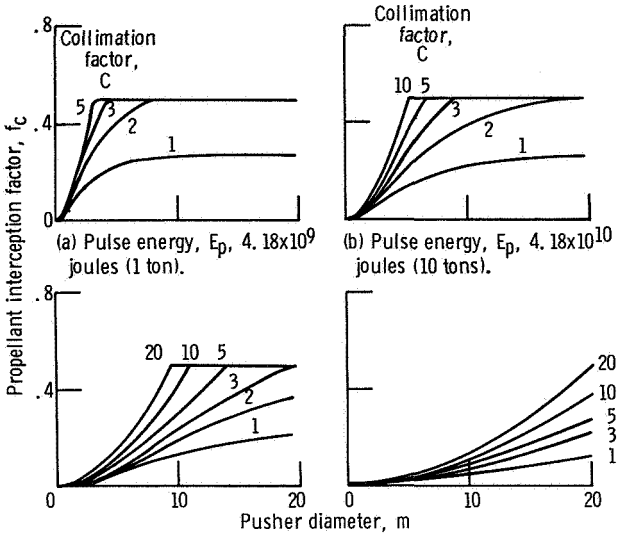

Figure 3. - Propellant interception factor variation with pusher diameter, pulse energy, and collimation factor.

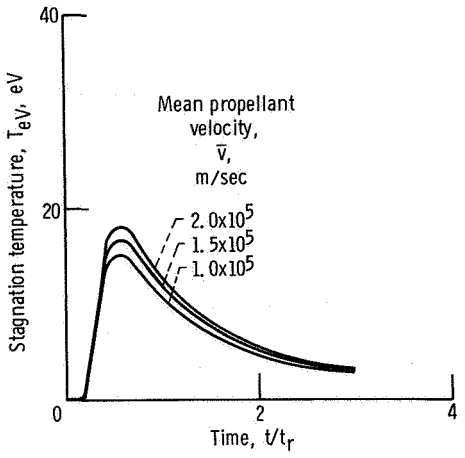

Figure 4. - Time variation of stagnation temperature.

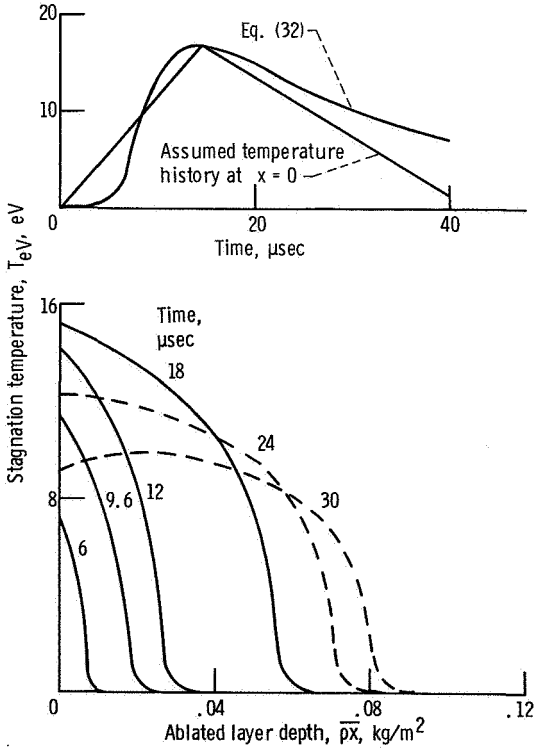

Figure 5. - Temperature profiles in ablated medium. Pulse energy, E_p, 4.18x10^{11} joules (100 tons); collimation factor, C, 3; mean propellant velocity, $\bar{v}$, 1.5x10^5 meters per second; absorption coefficient, a_R/ρ, 10^3 square meters per kilogram; thermal conductivity, k_c, 0.42 joule per meter per second per Kelvin degree.

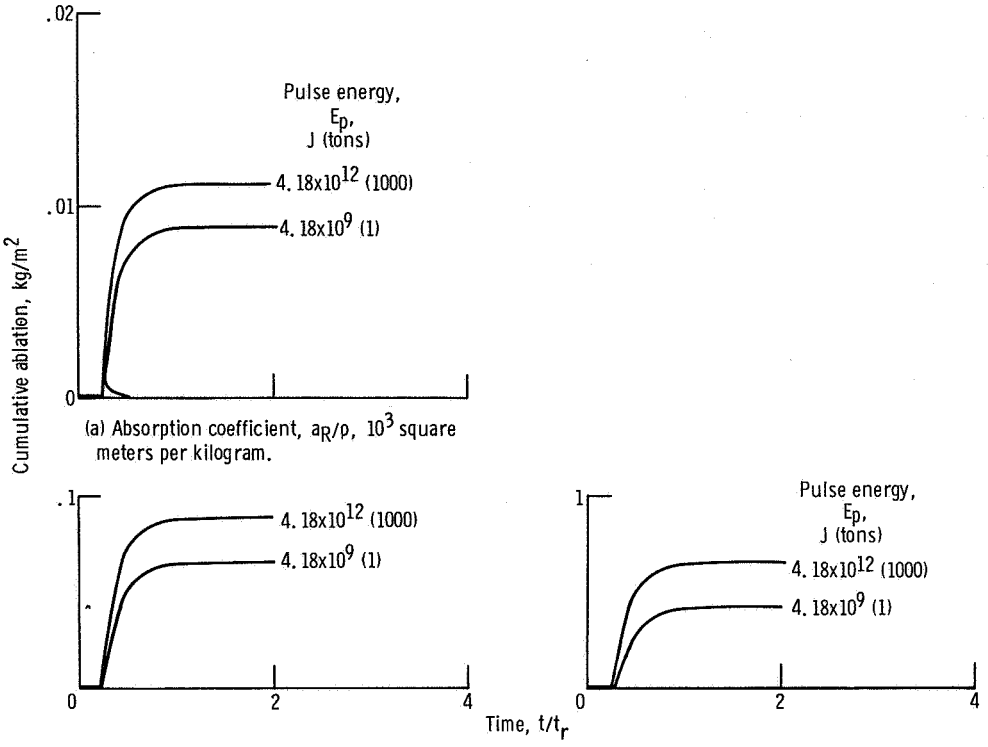

(a) Absorption coefficient, a_R/ρ, 10^3 square meters per kilogram.

(b) Absorption coefficient, a_R/ρ, 10^2 square meters per kilogram.

(c) Absorption coefficient, a_R/ρ, 10 square meters per kilogram.

Figure 6. - Cumulative ablation per unit area as function of time for an energy required to ablate pusher material H_a of $5x10^7$ joules per kilogram. Distance from pulse center equal to minimum radius, $r = r_m$; collimation factor, C, 3.

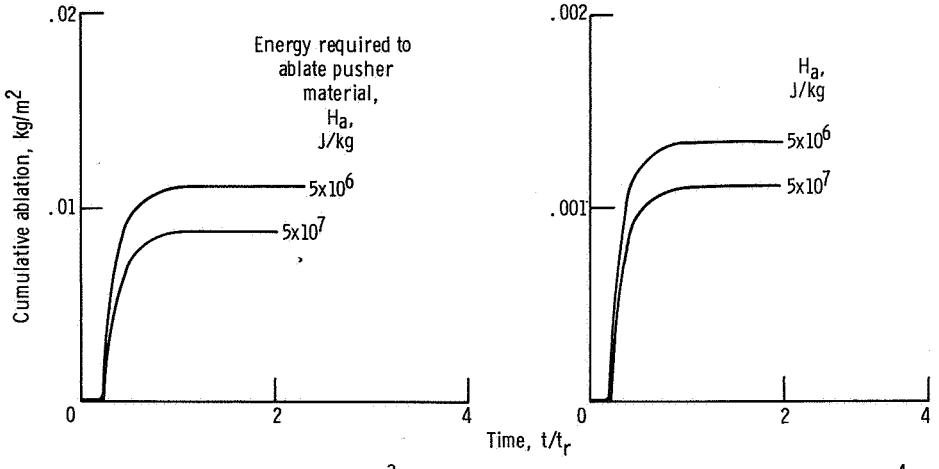

(a) Absorption coefficient, a_R/ρ, 10^3 square meters per kilogram.

(b) Absorption coefficient, a_R/ρ, 10^4 square meters per kilogram.

Figure 7. - Cumulative ablation per unit area as function of time for pulse energy E_p of $4.18x10^9$ joules (1 ton). Distance from pulse center equal to minimum radius, $r = r_m$; collimation factor, C, 3.

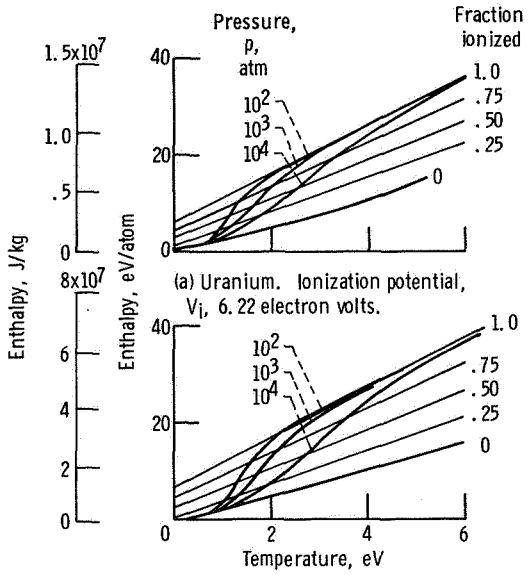

(a) Uranium. Ionization potential, V_i, 6.22 electron volts.

(b) Iron. Ionization potential, V_i, 7.87 electron volts.

Figure 8. - Enthalpy - temperature relation for two metal vapors.

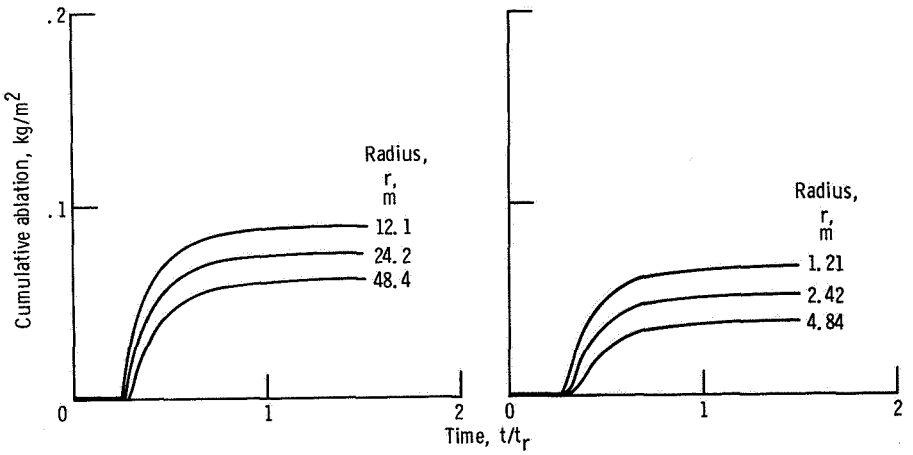

(a) Pulse energy, E_p, 4.18×10^{12} joules (1000 tons).

(b) Pulse energy, E_p, 4.18×10^9 joules (1 ton).

Figure 9. - Cumulative ablation per unit area as function of time for various separation distances. Absorption coefficient, a_R/ρ, 10^2 square meters per kilogram; energy required to ablate pusher material, H_a, 5×10^7 joules per kilogram.

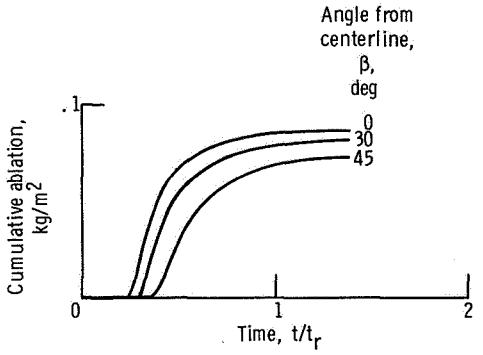

Figure 10. - Variation of cumulative ablation per unit area with time for various angles from centerline. Pulse energy, E_p, 4.18×10^9 joules (1 ton); distance from pulse center equal to minimum radius, $r = r_m$, 1.21 meters; absorption coefficient, a_R/ρ, 10^2 square meters per kilogram.

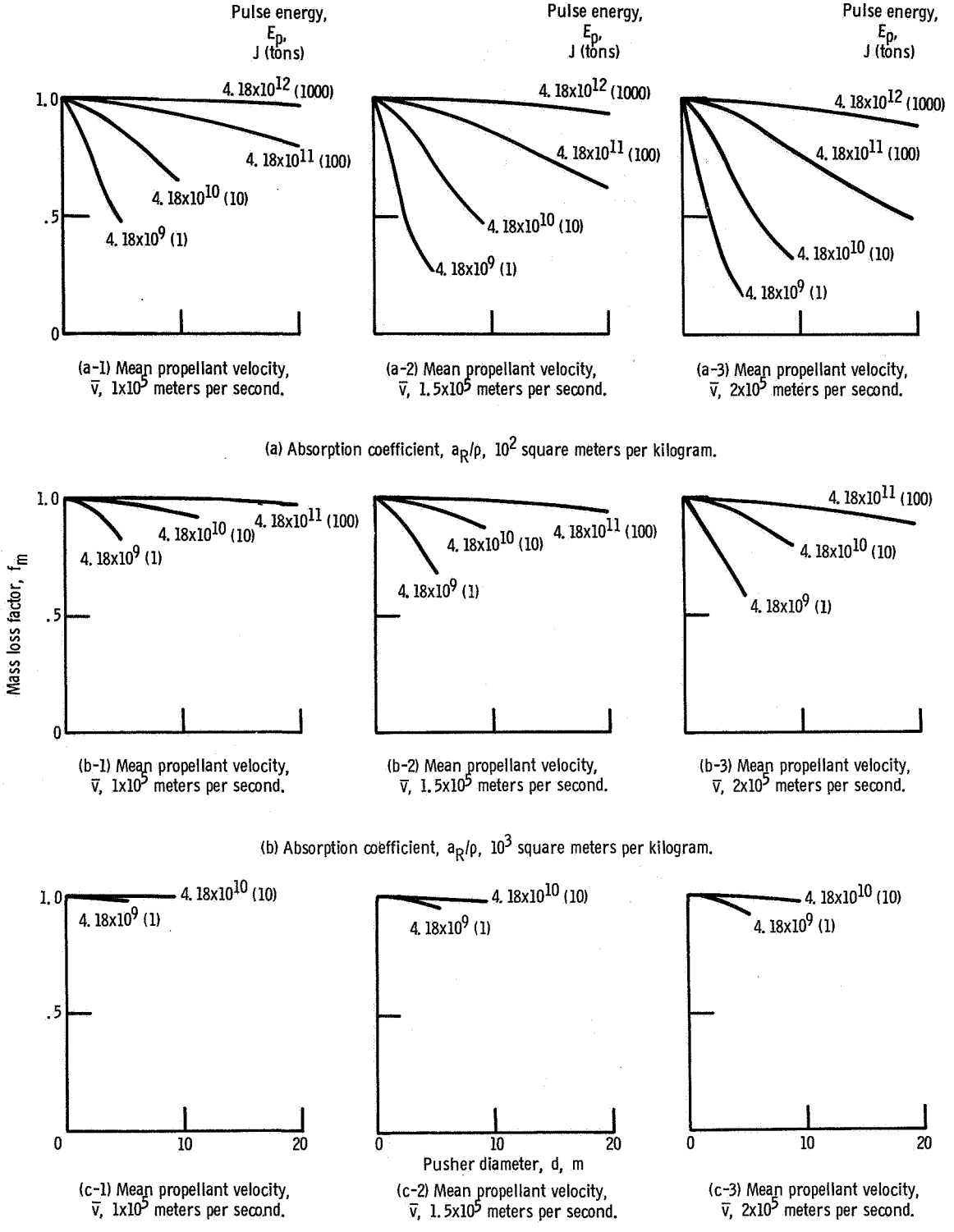

Figure 11. - Mass loss factor variation with pusher diameter, pulse energy, mean propellant velocity and opacity. Collimation factor, C, 3.

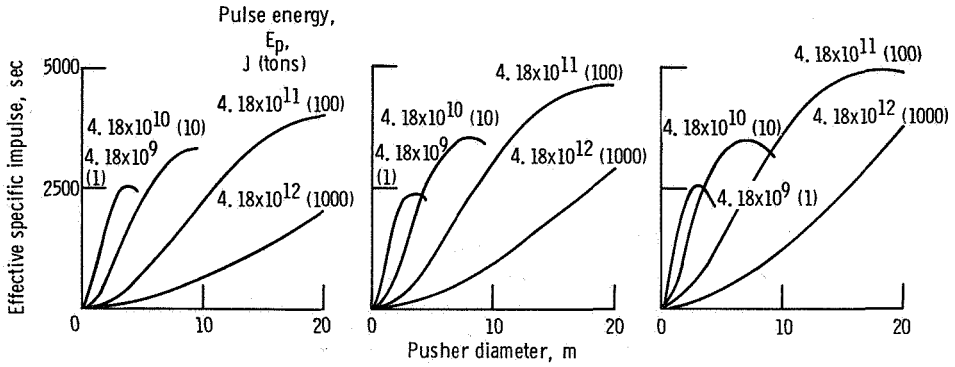

(a) Base specific impulse, $(I_{sp})_{base}$, 10 000 seconds.

(b) Base specific impulse, $(I_{sp})_{base}$, 15 000 seconds.

(c) Base specific impulse, $(I_{sp})_{base}$, 20 000 seconds.

Figure 12. - Effective specific impulse variation with pusher diameter, pulse energy, and mean propellant velocity. Collimation factor, C, 3; absorption coefficient, a_R/ρ, 10^2 square meters per kilogram.

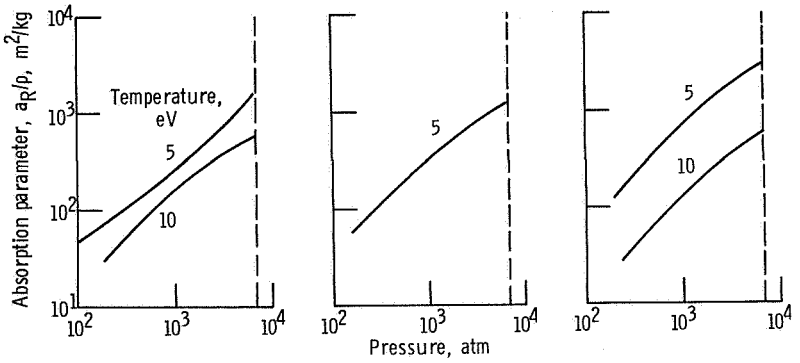

(a) Carbon.

(b) Beryllium.

(c) Hydrocarbon.

Figure 13. - Variation of absorption parameter with pressure and temperature for several materials.

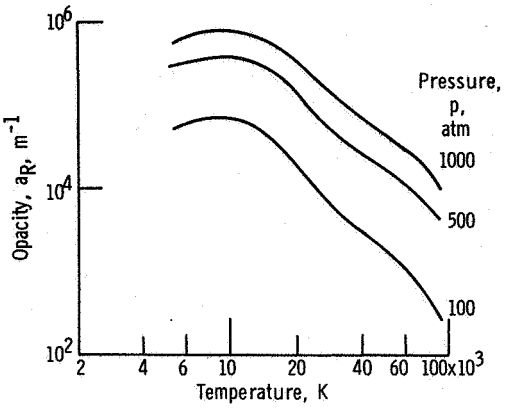

Figure 14. - Variation of Rosseland mean opacity of uranium with temperature and pressure.

NASA-Langley, 1972 —— 28 E-7013

"The aeronautical and space activities of the United States shall be conducted so as to contribute . . . to the expansion of human knowledge of phenomena in the atmosphere and space. The Administration shall provide for the widest practicable and appropriate dissemination of information concerning its activities and the results thereof."

—NATIONAL AERONAUTICS AND SPACE ACT OF 1958

NASA SCIENTIFIC AND TECHNICAL PUBLICATIONS

TECHNICAL REPORTS: Scientific and technical information considered important, complete, and a lasting contribution to existing knowledge.

TECHNICAL NOTES: Information less broad in scope but nevertheless of importance as a contribution to existing knowledge.

TECHNICAL MEMORANDUMS: Information receiving limited distribution because of preliminary data, security classification, or other reasons.

CONTRACTOR REPORTS: Scientific and technical information generated under a NASA contract or grant and considered an important contribution to existing knowledge.

TECHNICAL TRANSLATIONS: Information published in a foreign language considered to merit NASA distribution in English.

SPECIAL PUBLICATIONS: Information derived from or of value to NASA activities. Publications include conference proceedings, monographs, data compilations, handbooks, sourcebooks, and special bibliographies.

TECHNOLOGY UTILIZATION PUBLICATIONS: Information on technology used by NASA that may be of particular interest in commercial and other non-aerospace applications. Publications include Tech Briefs, Technology Utilization Reports and Technology Surveys.

Details on the availability of these publications may be obtained from:

SCIENTIFIC AND TECHNICAL INFORMATION OFFICE

NATIONAL AERONAUTICS AND SPACE ADMINISTRATION

Washington, D.C. 20546